Tolerance Analysis Through Interval Arithmetic in Reconfigurable Monopulse Antenna Arrays

N. Anselmi, P. Rocca, and A. Massa

2024/12/13

Contents

1 Performances Analysis: a fair comparison

In order to prove the criticality of the common elements in terms of radiation performances of the reconfigurable system, a more fair comparison is needed. Towards this end we need to fix the number of faulty elements in this manner:

- $F = P$ faulty common elements;
- $F = P$ faulty elements among the Q not-common elements;

remembering that P is the number of common elements.

Also in this case, in order to model manufacturing errors, faults and failures, **maximum widths** intervals are used, that is, considering normalized amplitudes, the n-th faulty common/not-common element's interval amplitude is equal to:

$$\mathbf{A}_n = [0.0,\ 1.0] \tag{1}$$

Several reconfigurable antenna arrays affording sum and a difference patterns are considered, with different number of common control points:

- $P = 2,\ 4,\ 6,\ 8$

For each test case, intervals are applied only over common amplitudes ($\mathbf{A}_n^C$) and then only over not-common amplitudes ($\mathbf{A}_n^{NC}$) .

Common Faulty Elements Analysis:

- In this case the amplitude intervals are considered over all the $F = P$ common elements (Figure 2).
- For each case the interval pattern $\mathbf{P}$ and the $\mathbf{SLL}$ and $\mathbf{BW}$ intervals are computed.

Not-Common Faulty Elements Analysis:

In this case we must consider three different scenarios:

- the $F = P$ faulty elements belong to the Σ beam's feeding network;
- the $F = P$ faulty elements belong to the Δ beam's feeding network;
- the $F = P$ faulty elements belong half to the Σ beam's feeding network and half to the Δ feeding network (Figure 5).

Then for each scenario:

- we must consider all the $\begin{pmatrix} Q \\ P \end{pmatrix}$ combinations of P faulty elements among the Q not-common elements;
- for each combination the interval pattern $\mathbf{P}$ and the $\mathbf{SLL}$ and $\mathbf{BW}$ intervals are computed.

Auxiliary Definitions:

In order to better compare the results of this section we define:

- $$\zeta_{\{\cdot\}} = \sup\{\cdot\}_{max} - \inf\{\cdot\}_{min} \tag{2}$$

- $$\chi_{\{\cdot\}} = \left(\sup\{\cdot\}^{\Sigma}_{max} - \inf\{\cdot\}^{\Sigma}_{min}\right) + \left(\sup\{\cdot\}^{\Delta}_{max} - \inf\{\cdot\}^{\Delta}_{min}\right) \tag{3}$$

where $\sup$ / $\inf\{\cdot\}_{max}$ is the maximum $\sup$ / $\inf$ among all the considered combination of faulty elements; $\sup$ / $\inf\{\cdot\}_{min}$ is the respective minimum value.

1.1 Faulty elements over Σ beam's feeding network

In the following figures the **BLUE** line refers to the common faulty elements analysis. As regards the not-common faulty elements analysis, only the minimum $\inf\{\mathbf{SLL}\}$ and the maximum $\sup\{\mathbf{SLL}\}$ are traced (**RED** lines), while all the other possible bounds are contained into the **PINK** area.

SLL:

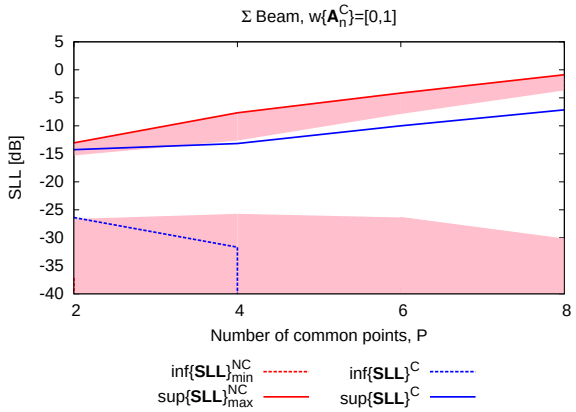

Figure 1. Sum Pattern **SLL** vs P

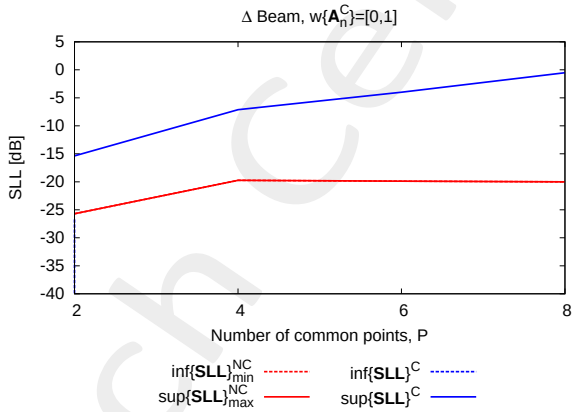

Figure 2. Difference Pattern **SLL** vs P

P	$\inf\{\mathbf{SLL}\}^C$	$\sup\{\mathbf{SLL}\}^C$	$\inf\{\mathbf{SLL}\}^{NC}_{min}$	$\inf\{\mathbf{SLL}\}^{NC}_{max}$	$\sup\{\mathbf{SLL}\}^{NC}_{min}$	$\sup\{\mathbf{SLL}\}^{NC}_{max}$
2	-26.37	-14.26	-37.17	-26.63	-15.3	-13.05
4	-31.68	-13.16	$-\infty$	-25.72	-12.63	-7.67
6	$-\infty$	-10.0	$-\infty$	-26.36	-7.89	-4.15
8	$-\infty$	-7.15	$-\infty$	-30.21	-3.67	-0.89

Table 1. Sum Pattern **SLL** values

P	$\inf\{\mathbf{SLL}\}^C$	$\sup\{\mathbf{SLL}\}^C$	$\inf\{\mathbf{SLL}\}^{NC}_{min}$	$\inf\{\mathbf{SLL}\}^{NC}_{max}$	$\sup\{\mathbf{SLL}\}^{NC}_{min}$	$\sup\{\mathbf{SLL}\}^{NC}_{max}$
2	-26.71	-15.37	-25.7	-25.7	-25.7	-25.7
4	$-\infty$	-7.11	-19.74	-19.74	-19.74	-19.74
6	$-\infty$	-4.0	-19.88	-19.88	-19.88	-19.88
8	$-\infty$	-0.52	-20.01	-20.01	-20.01	-20.01

Table 2. Difference Pattern **SLL** values

WORST CASES:

In the following the patterns and excitations of the worst cases in terms of $\sup\{\mathbf{SLL}\}_{max}^{NC}$ are reported.

- $P = 2$

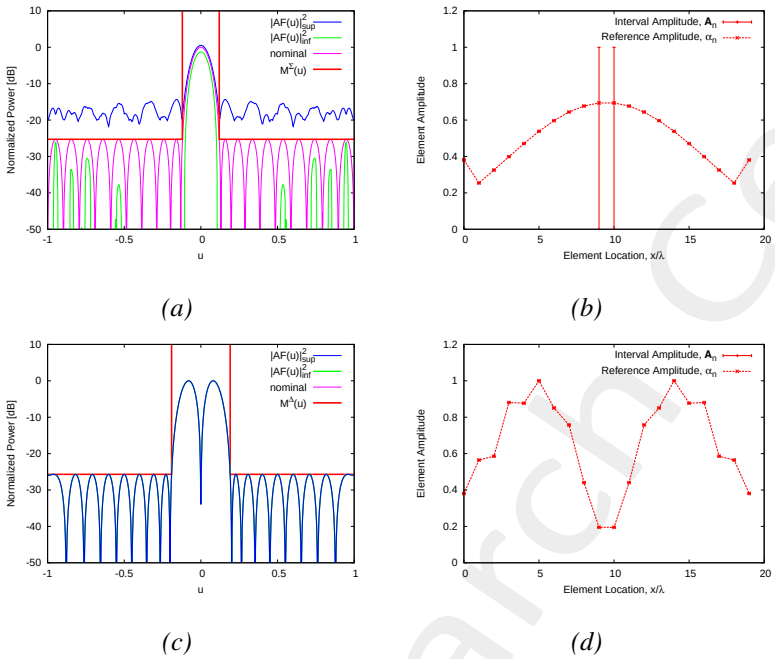

(a) *(b)*

(c) *(d)*

Figure 3. Radiation patterns *(a)(c)* and amplitudes *(b)(d)* for the worst sum beam *(a)(b)* and difference beam *(c)(d)* in terms of SLL.

- $P = 4$

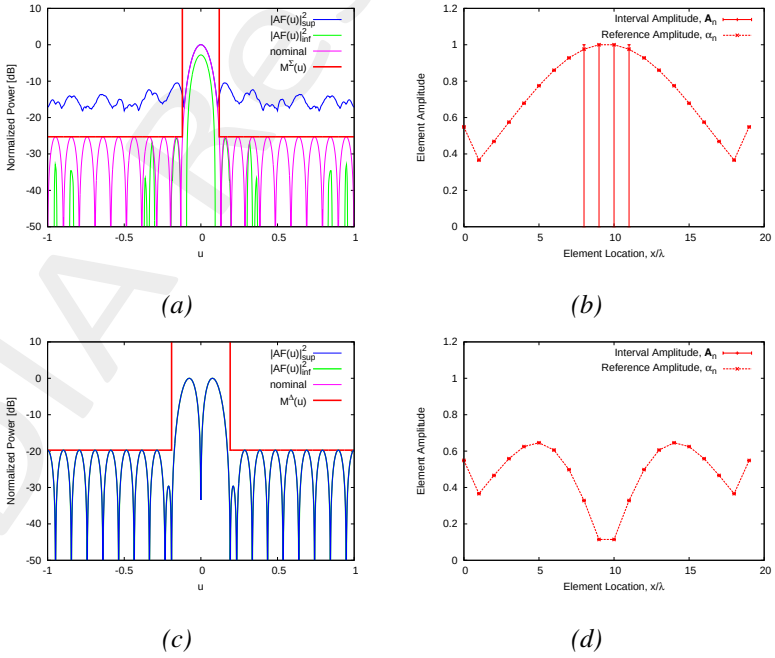

(a) *(b)*

(c) *(d)*

Figure 4. Radiation patterns *(a)(c)* and amplitudes *(b)(d)* for the worst sum beam *(a)(b)* and difference beam *(c)(d)* in terms of SLL.

- $P = 6$

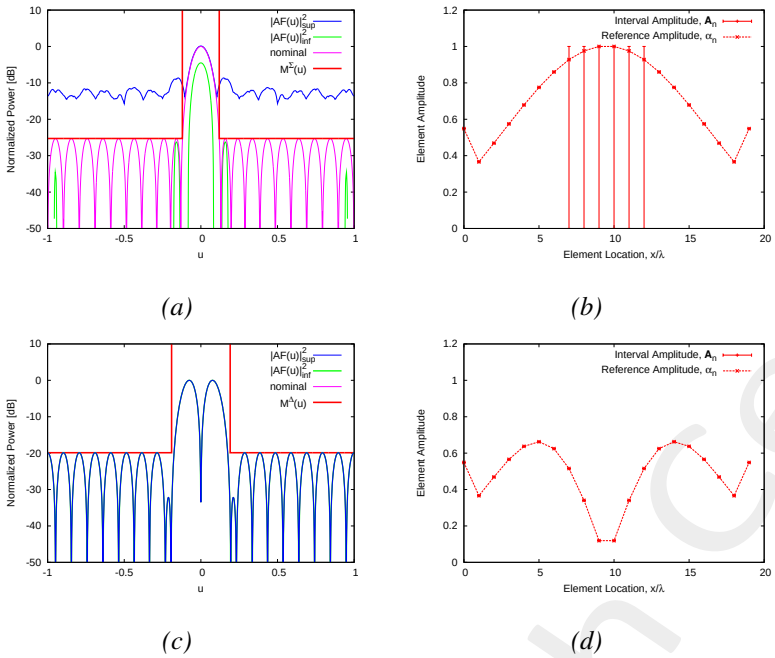

(a) *(b)*

(c) *(d)*

Figure 5. Radiation patterns *(a)(c)* and amplitudes *(b)(d)* for the worst sum beam *(a)(b)* and difference beam *(c)(d)* in terms of SLL.

- $P = 8$

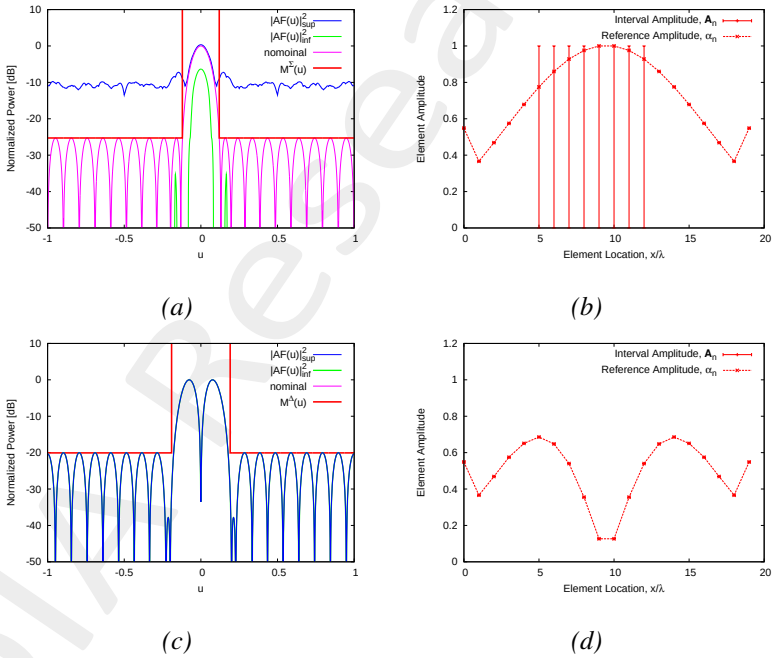

(a) *(b)*

(c) *(d)*

Figure 6. Radiation patterns *(a)(c)* and amplitudes *(b)(d)* for the worst sum beam *(a)(b)* and difference beam *(c)(d)* in terms of SLL.

BW:

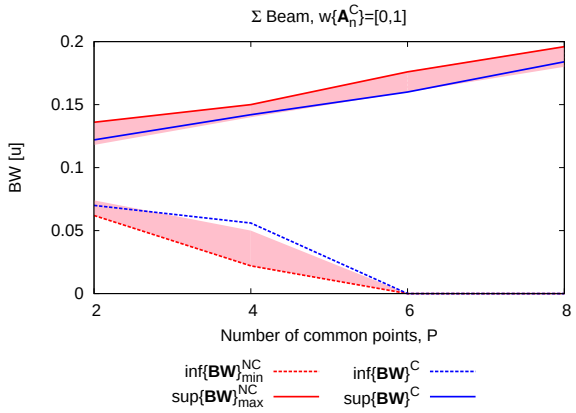

Figure 7. Sum Pattern $\mathbf{BW}$ vs P

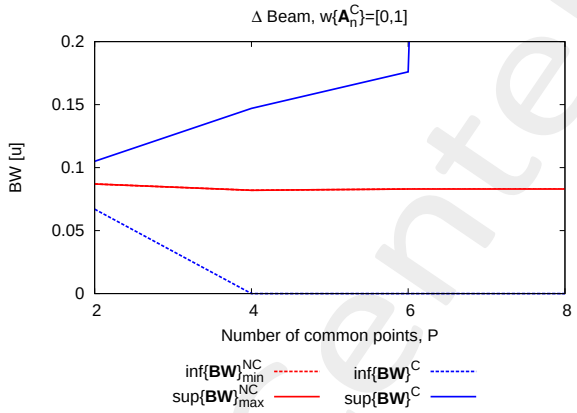

Figure 8. Difference Pattern $\mathbf{BW}$ vs P

P	$\inf\{\mathbf{BW}\}^{C}$	$\sup\{\mathbf{BW}\}^{C}$	$\inf\{\mathbf{BW}\}^{NC}_{min}$	$\inf\{\mathbf{BW}\}^{NC}_{max}$	$\sup\{\mathbf{BW}\}^{NC}_{min}$	$\sup\{\mathbf{BW}\}^{NC}_{max}$
2	0.07	0.122	0.062	0.074	0.118	0.136
4	0.056	0.142	0.022	0.05	0.14	0.15
6	0.0	0.16	0.0	0.0	0.16	0.176
8	0.0	0.184	0.0	0.0	0.18	0.196

Table 3. Sum Pattern $\mathbf{BW}$ values

P	$\inf\{\mathbf{BW}\}^{C}$	$\sup\{\mathbf{BW}\}^{C}$	$\inf\{\mathbf{BW}\}^{NC}_{min}$	$\inf\{\mathbf{BW}\}^{NC}_{max}$	$\sup\{\mathbf{BW}\}^{NC}_{min}$	$\sup\{\mathbf{BW}\}^{NC}_{max}$
2	0.067	0.105	0.087	0.087	0.087	0.087
4	0.0	0.147	0.082	0.082	0.082	0.082
6	0.0	0.176	0.083	0.083	0.083	0.083
8	0.0	4.0	0.083	0.083	0.083	0.083

Table 4. Difference Pattern $\mathbf{BW}$ values

WORST CASES:

In the following the patterns and excitations of the worst cases in terms of $\sup\{\mathbf{BW}\}_{max}^{NC}$ are reported.

- $P = 2$

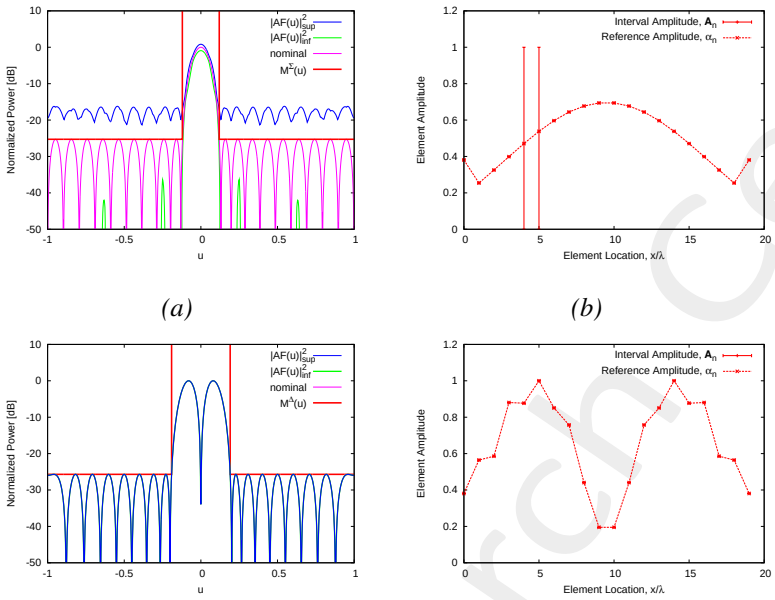

(a) *(b)*

(c) *(d)*

Figure 9. Radiation patterns *(a)(c)* and amplitudes *(b)(d)* for the worst sum beam *(a)(b)* and difference beam *(c)(d)* in terms of BW.

- $P = 4$

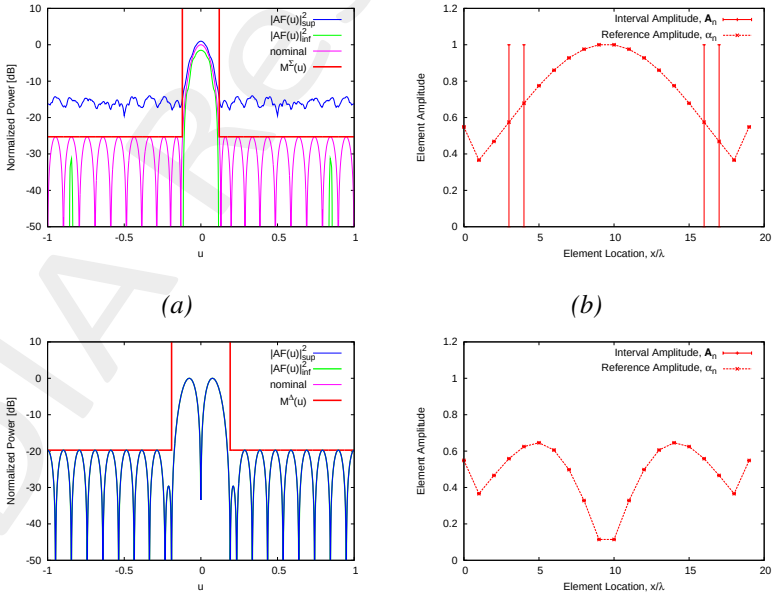

(a) *(b)*

(c) *(d)*

Figure 10. Radiation patterns *(a)(c)* and amplitudes *(b)(d)* for the worst sum beam *(a)(b)* and difference beam *(c)(d)* in terms of BW.

- $P = 6$

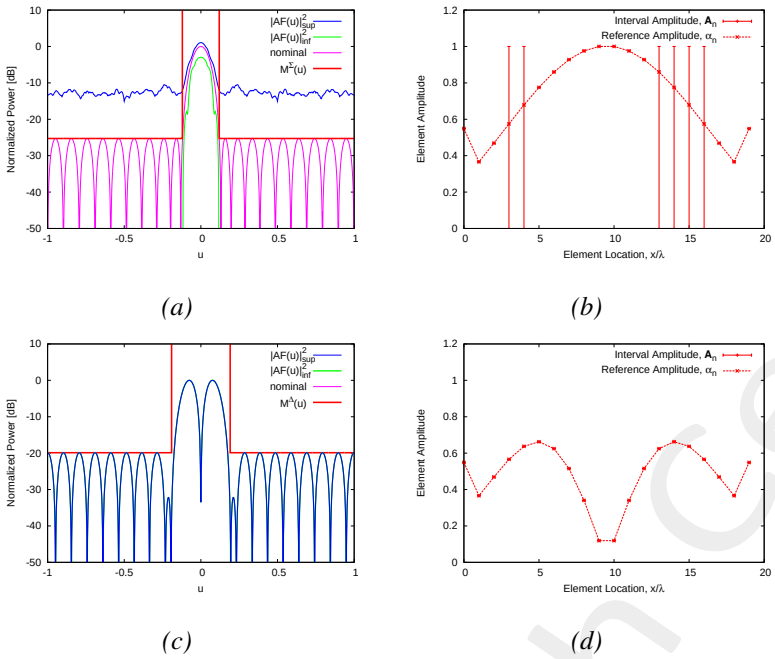

(a) *(b)*

(c) *(d)*

Figure 11. Radiation patterns *(a)(c)* and amplitudes *(b)(d)* for the worst sum beam *(a)(b)* and difference beam *(c)(d)* in terms of BW.

- $P = 8$

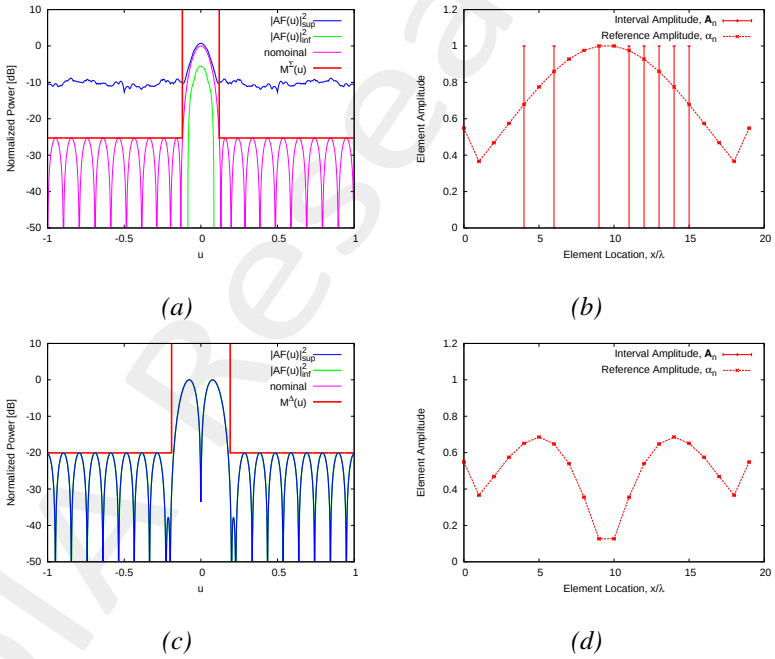

(a) *(b)*

(c) *(d)*

Figure 12. Radiation patterns *(a)(c)* and amplitudes *(b)(d)* for the worst sum beam *(a)(b)* and difference beam *(c)(d)* in terms of BW.

Remembering that:

- $$\chi_{\{\cdot\}} = \left(\sup\{\cdot\}^{\Sigma}_{max} - \inf\{\cdot\}^{\Sigma}_{min}\right) + \left(\sup\{\cdot\}^{\Delta}_{max} - \inf\{\cdot\}^{\Delta}_{min}\right) \quad (4)$$

where $\sup / \inf\{\cdot\}_{max}$ is the maximum $\sup / \inf$ among all the considered combination of faulty elements; $\sup / \inf\{\cdot\}_{min}$ is the respective minimum value.

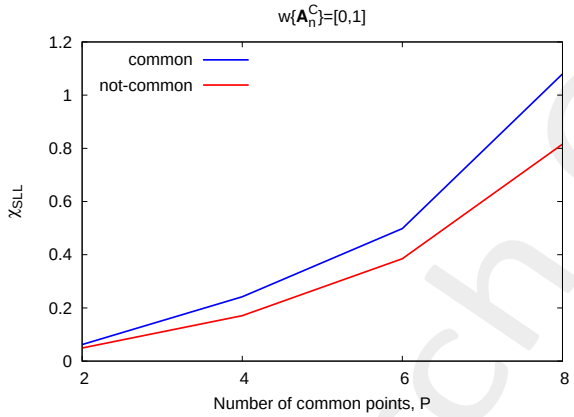

Figure 13. The χ_{SLL} relative to the SLL descriptor is plotted, for the common and not-common cases

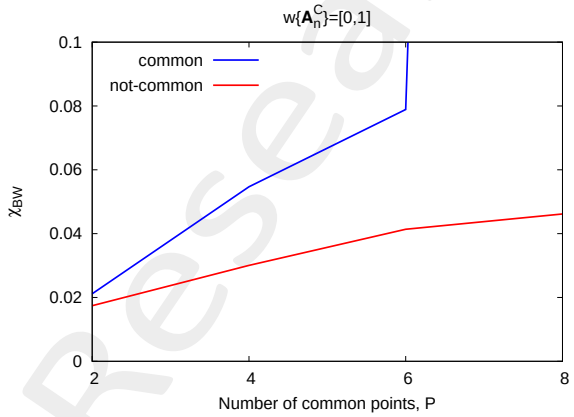

Figure 14. The χ_{BW} relative to the BW descriptor is plotted, for the common and not-common cases

Observations:

- The criticality of common elements is well showed by the above Figures 6 and 7.
- Parameters χ_{SLL} and χ_{BW} trends show that in this case the sum of the tolerances on the Σ and Δ beams of the respective descriptors is always major in case of common faulty elements with respect to independent faulty elements.

1.2 Faulty elements over Δ beam's feeding network

SLL:

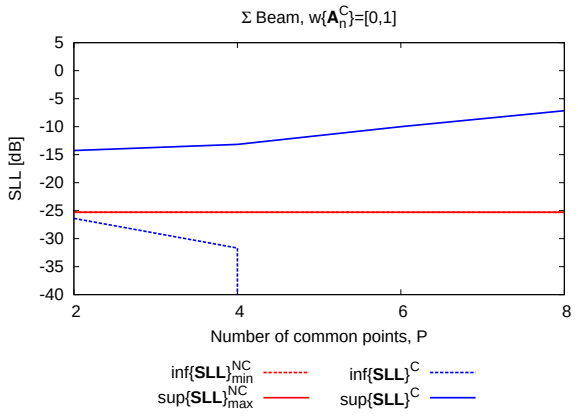

Figure 15. Sum Pattern **SLL** vs P

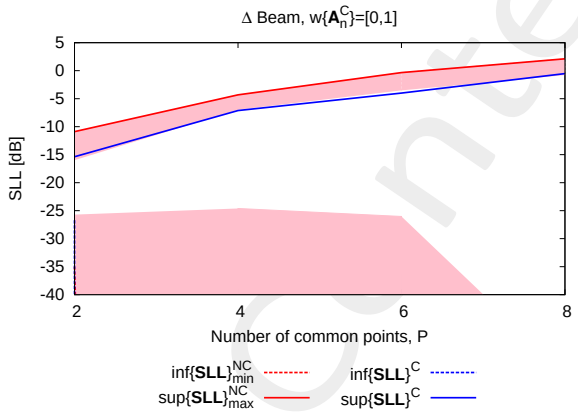

Figure 16. Difference Pattern **SLL** vs P

P	$\inf\{\mathbf{SLL}\}^{C}$	$\sup\{\mathbf{SLL}\}^{C}$	$\inf\{\mathbf{SLL}\}_{min}^{NC}$	$\inf\{\mathbf{SLL}\}_{max}^{NC}$	$\sup\{\mathbf{SLL}\}_{min}^{NC}$	$\sup\{\mathbf{SLL}\}_{max}^{NC}$
2	-26.37	-14.26	-25.28	-25.28	-25.28	-25.28
4	-31.68	-13.16	-25.28	-25.28	-25.28	-25.28
6	$-\infty$	-10.0	-25.28	-25.28	-25.28	-25.28
8	$-\infty$	-7.15	-25.28	-25.28	-25.28	-25.28

Table 1. Sum Pattern **SLL** values

P	$\inf\{\mathbf{SLL}\}^{C}$	$\sup\{\mathbf{SLL}\}^{C}$	$\inf\{\mathbf{SLL}\}_{min}^{NC}$	$\inf\{\mathbf{SLL}\}_{max}^{NC}$	$\sup\{\mathbf{SLL}\}_{min}^{NC}$	$\sup\{\mathbf{SLL}\}_{max}^{NC}$
2	-26.71	-15.37	-35.0	-25.7	-15.99	-10.88
4	$-\infty$	-7.11	$-\infty$	-24.61	-6.97	-4.31
6	$-\infty$	-4.0	$-\infty$	-26.03	-3.52	-0.34
8	$-\infty$	-0.52	$-\infty$	-53.88	-0.79	2.12

Table 2. Difference Pattern **SLL** values

WORST CASES:

In the following the patterns and excitations of the worst cases in terms of $\sup\{\mathbf{SLL}\}_{max}^{NC}$ are reported.

- $P = 2$

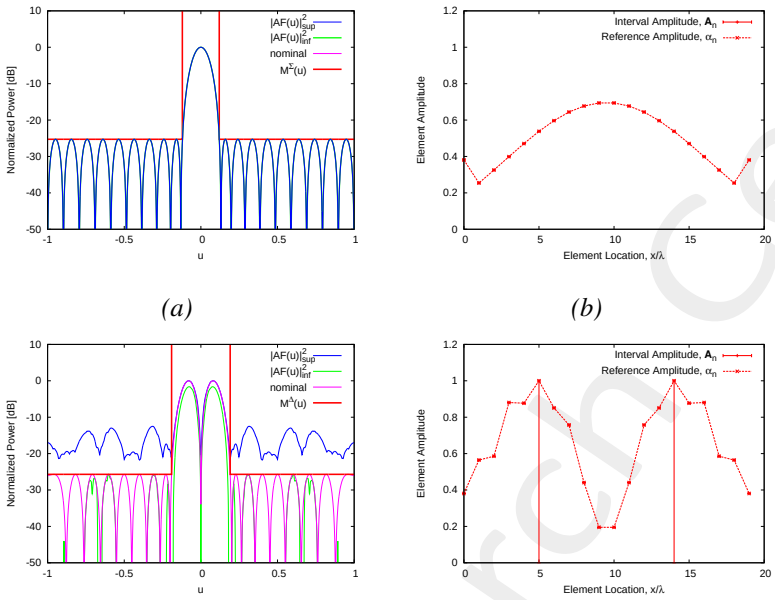

Figure 17. Radiation patterns *(a)(c)* and amplitudes *(b)(d)* for the worst sum beam *(a)(b)* and difference beam *(c)(d)* in terms of SLL.

- $P = 4$

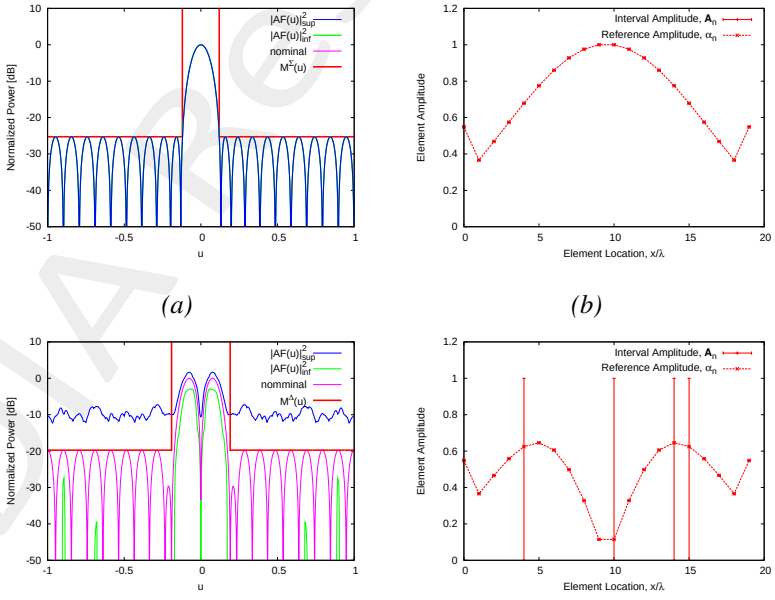

Figure 18. Radiation patterns *(a)(c)* and amplitudes *(b)(d)* for the worst sum beam *(a)(b)* and difference beam *(c)(d)* in terms of SLL.

- $P = 6$

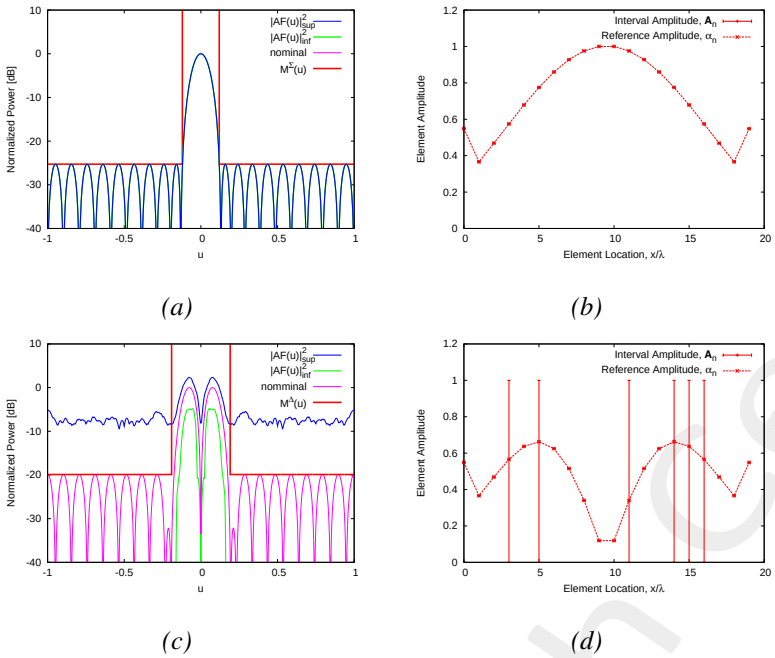

(a) *(b)*

(c) *(d)*

Figure 19. Radiation patterns *(a)(c)* and amplitudes *(b)(d)* for the worst sum beam *(a)(b)* and difference beam *(c)(d)* in terms of SLL.

- $P = 8$

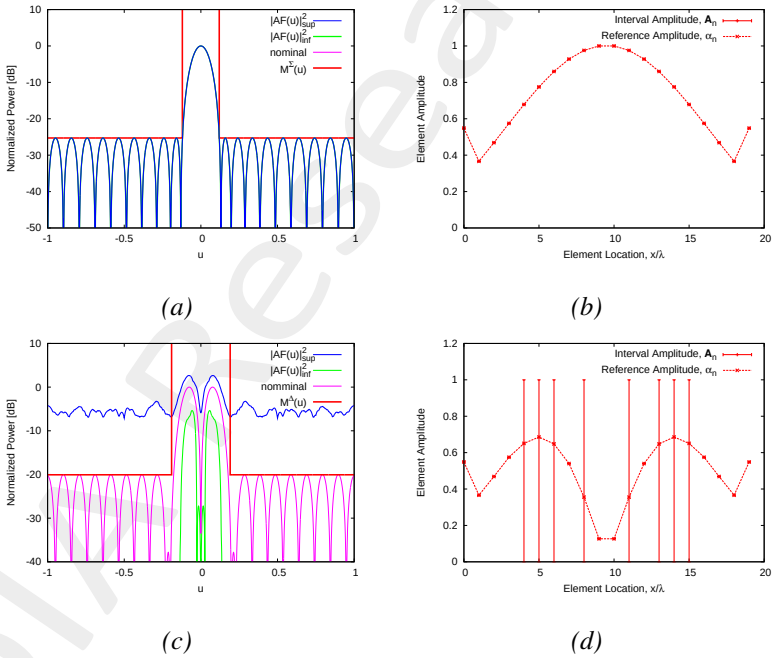

(a) *(b)*

(c) *(d)*

Figure 20. Radiation patterns *(a)(c)* and amplitudes *(b)(d)* for the worst sum beam *(a)(b)* and difference beam *(c)(d)* in terms of SLL.

BW:

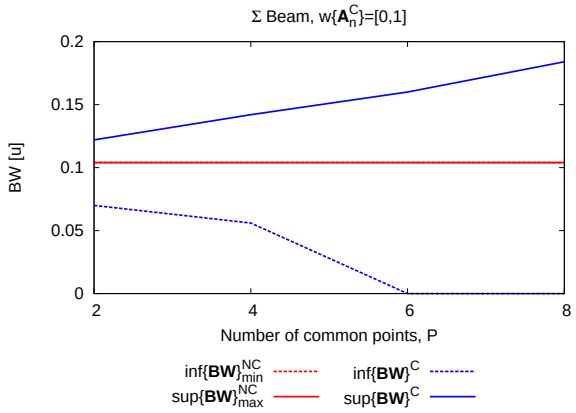

Figure 21. Sum Pattern $\mathbf{BW}$ vs P

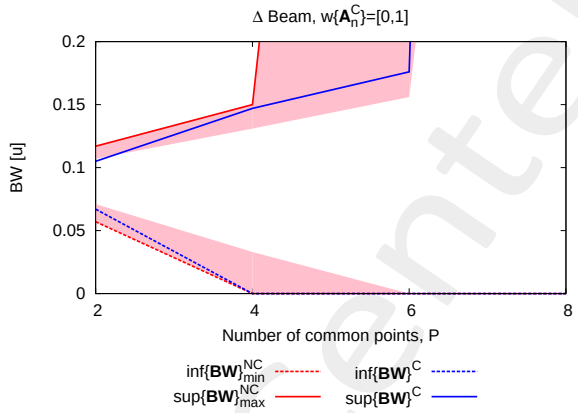

Figure 22. Difference Pattern $\mathbf{BW}$ vs P

P	$\inf\{\mathbf{BW}\}^{C}$	$\sup\{\mathbf{BW}\}^{C}$	$\inf\{\mathbf{BW}\}^{NC}_{min}$	$\inf\{\mathbf{BW}\}^{NC}_{max}$	$\sup\{\mathbf{BW}\}^{NC}_{min}$	$\sup\{\mathbf{BW}\}^{NC}_{max}$
2	0.07	0.122	0.104	0.104	0.104	0.104
4	0.056	0.142	0.104	0.104	0.104	0.104
6	0.0	0.16	0.104	0.104	0.104	0.104
8	0.0	0.184	0.104	0.104	0.104	0.104

Table 3. Sum Pattern $\mathbf{BW}$ values

P	$\inf\{\mathbf{BW}\}^{C}$	$\sup\{\mathbf{BW}\}^{C}$	$\inf\{\mathbf{BW}\}^{NC}_{min}$	$\inf\{\mathbf{BW}\}^{NC}_{max}$	$\sup\{\mathbf{BW}\}^{NC}_{min}$	$\sup\{\mathbf{BW}\}^{NC}_{max}$
2	0.067	0.105	0.057	0.071	0.107	0.117
4	0.0	0.147	0.0	0.033	0.131	0.15
6	0.0	0.176	0.0	0.0	0.156	1.266
8	0.0	4.0	0.0	0.0	1.2	4.0

Table 4. Difference Pattern $\mathbf{BW}$ values

WORST CASES:

In the following the patterns and excitations of the worst cases in terms of $\sup\{\mathbf{BW}\}_{max}^{NC}$ are reported.

- $P = 2$

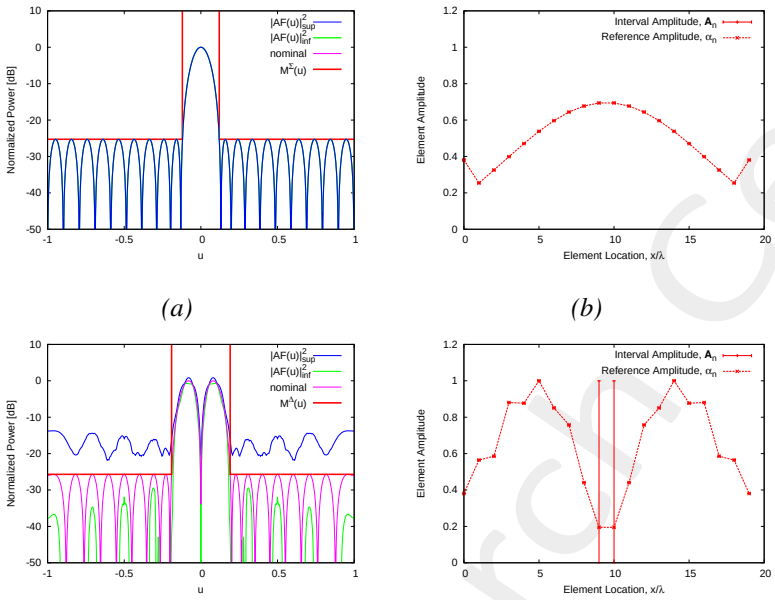

(a) *(b)*

(c) *(d)*

Figure 23. Radiation patterns *(a)(c)* and amplitudes *(b)(d)* for the worst sum beam *(a)(b)* and difference beam *(c)(d)* in terms of BW.

- $P = 4$

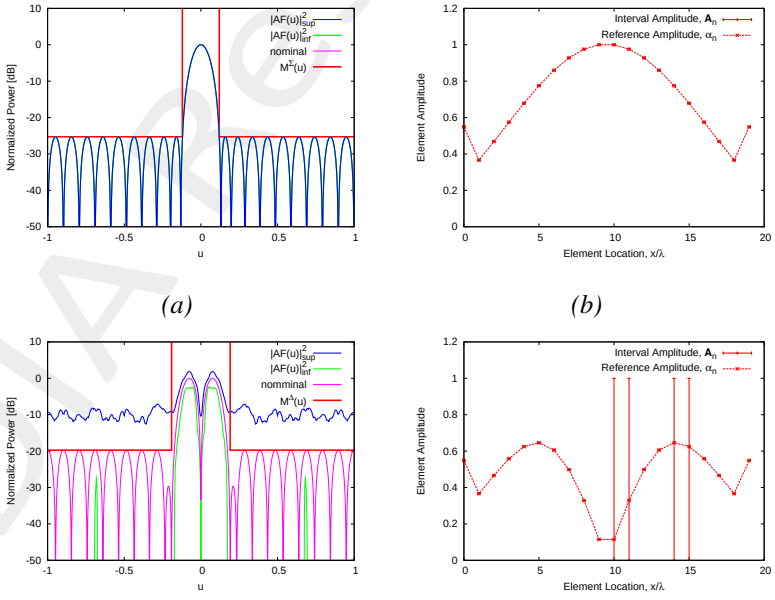

(a) *(b)*

(c) *(d)*

Figure 24. Radiation patterns *(a)(c)* and amplitudes *(b)(d)* for the worst sum beam *(a)(b)* and difference beam *(c)(d)* in terms of BW.

- $P = 6$

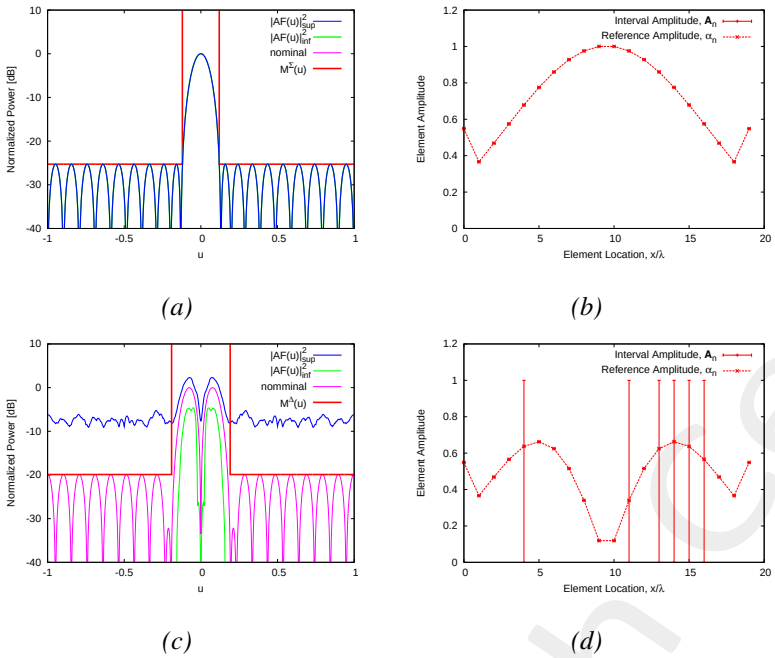

Figure 25. Radiation patterns *(a)(c)* and amplitudes *(b)(d)* for the worst sum beam *(a)(b)* and difference beam *(c)(d)* in terms of BW.

Remembering that:

- $$\chi_{\{\cdot\}} = \left(\sup\{\cdot\}^{\Sigma}_{max} - \inf\{\cdot\}^{\Sigma}_{min}\right) + \left(\sup\{\cdot\}^{\Delta}_{max} - \inf\{\cdot\}^{\Delta}_{min}\right) \quad (5)$$

where $\sup / \inf\{\cdot\}_{max}$ is the maximum $\sup / \inf$ among all the considered combination of faulty elements; $\sup / \inf\{\cdot\}_{min}$ is the respective minimum value.

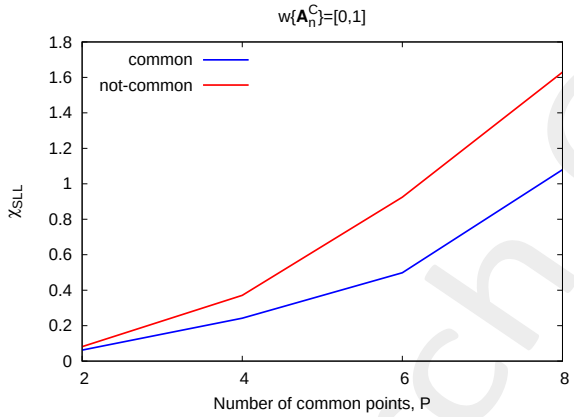

Figure 26. The χ_{SLL} relative to the SLL descriptor is plotted, for the common and not-common cases

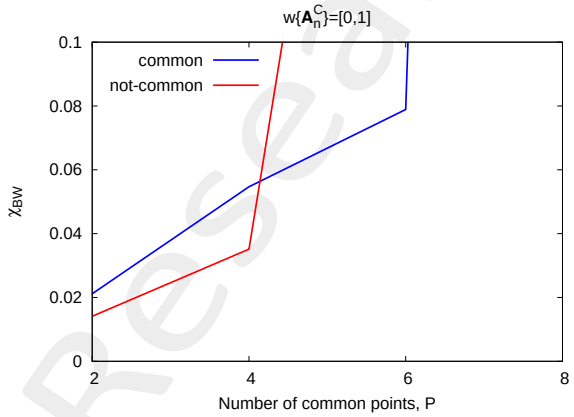

Figure 27. The χ_{BW} relative to the BW descriptor is plotted, for the common and not-common cases

Observations:

- In this case parameters χ_{SLL} and χ_{BW} trends show that the sum of the tolerances on the Σ and Δ beams of the respective descriptors is major when we are considering faulty elements on the independent Δ beam forming network. This can by explained by the compromise synthesis of the Δ beam, due to the fixed common elements.

1.3 Faulty elements over Σ and Δ beam's feeding network

SLL:

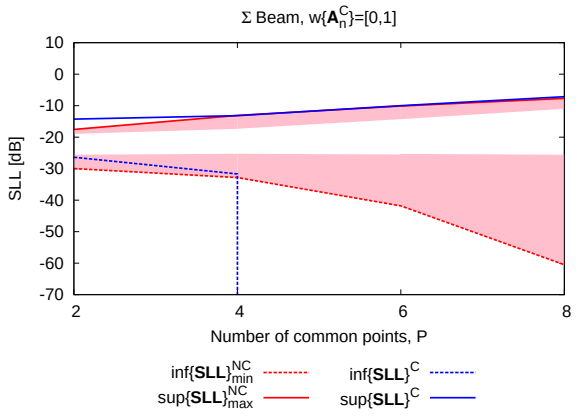

Figure 28. Sum Pattern **SLL** vs P

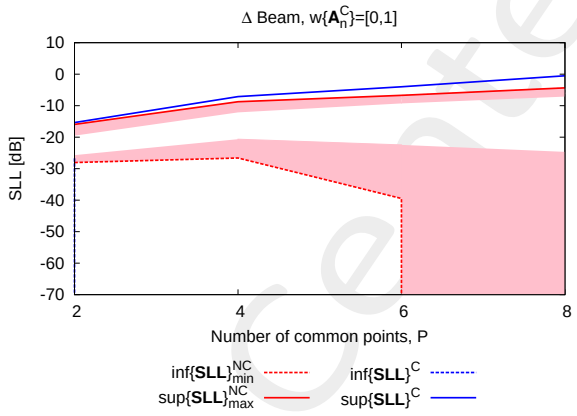

Figure 29. Difference Pattern **SLL** vs P

P	$\inf\{\mathbf{SLL}\}^{C}$	$\sup\{\mathbf{SLL}\}^{C}$	$\inf\{\mathbf{SLL}\}_{min}^{NC}$	$\inf\{\mathbf{SLL}\}_{max}^{NC}$	$\sup\{\mathbf{SLL}\}_{min}^{NC}$	$\sup\{\mathbf{SLL}\}_{max}^{NC}$
2	-26.37	-14.26	-29.97	-25.58	-18.97	-17.56
4	-31.68	-13.16	-32.82	-25.28	-17.32	-13.09
6	$-\infty$	-10.0	-41.82	-25.49	-14.28	-10.1
8	$-\infty$	-7.15	-60.51	-25.72	-11.0	-7.68

Table 1. Sum Pattern **SLL** values

P	$\inf\{\mathbf{SLL}\}^{C}$	$\sup\{\mathbf{SLL}\}^{C}$	$\inf\{\mathbf{SLL}\}_{min}^{NC}$	$\inf\{\mathbf{SLL}\}_{max}^{NC}$	$\sup\{\mathbf{SLL}\}_{min}^{NC}$	$\sup\{\mathbf{SLL}\}_{max}^{NC}$
2	-26.71	-15.37	-28.05	-25.7	-19.51	-15.95
4	$-\infty$	-7.11	-26.62	-20.63	-12.13	-8.74
6	$-\infty$	-4.0	-39.45	-22.45	-9.28	-6.72
8	$-\infty$	-0.52	$-\infty$	-24.68	-7.12	-4.35

Table 2. Difference Pattern **SLL** values

WORST CASES:

In the following the patterns and excitations of the worst cases in terms of $\sup\{\mathbf{SLL}\}_{max}^{NC}$ are reported.

- $P = 2$

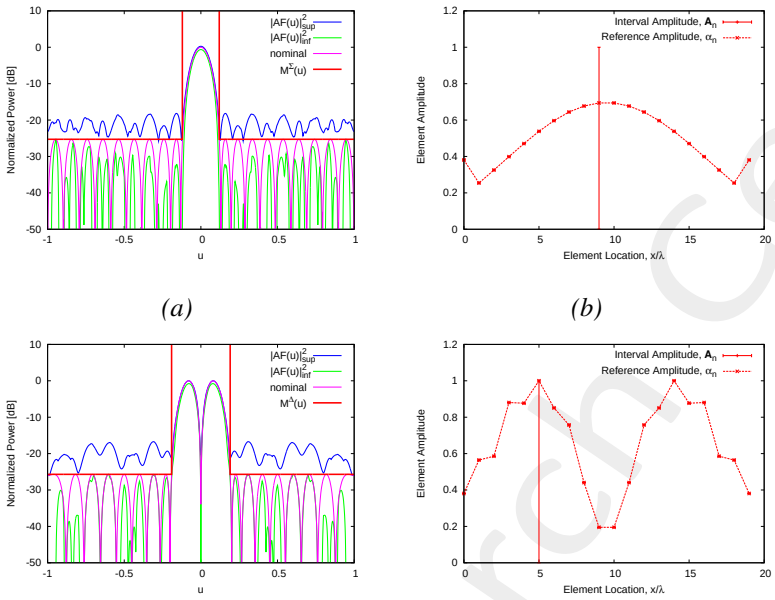

(a) *(b)*

(c) *(d)*

Figure 30. Radiation patterns *(a)(c)* and amplitudes *(b)(d)* for the worst sum beam *(a)(b)* and difference beam *(c)(d)* in terms of SLL.

- $P = 4$

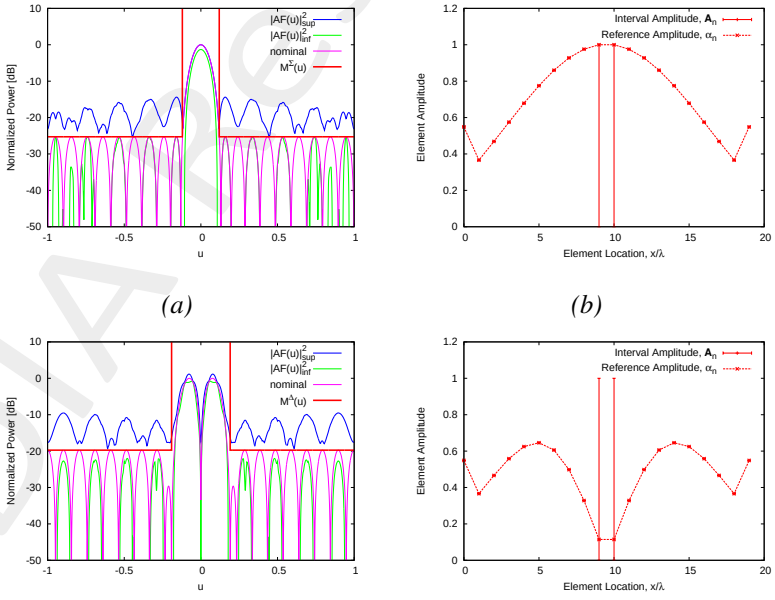

(a) *(b)*

(c) *(d)*

Figure 31. Radiation patterns *(a)(c)* and amplitudes *(b)(d)* for the worst sum beam *(a)(b)* and difference beam *(c)(d)* in terms of SLL.

- $P = 6$

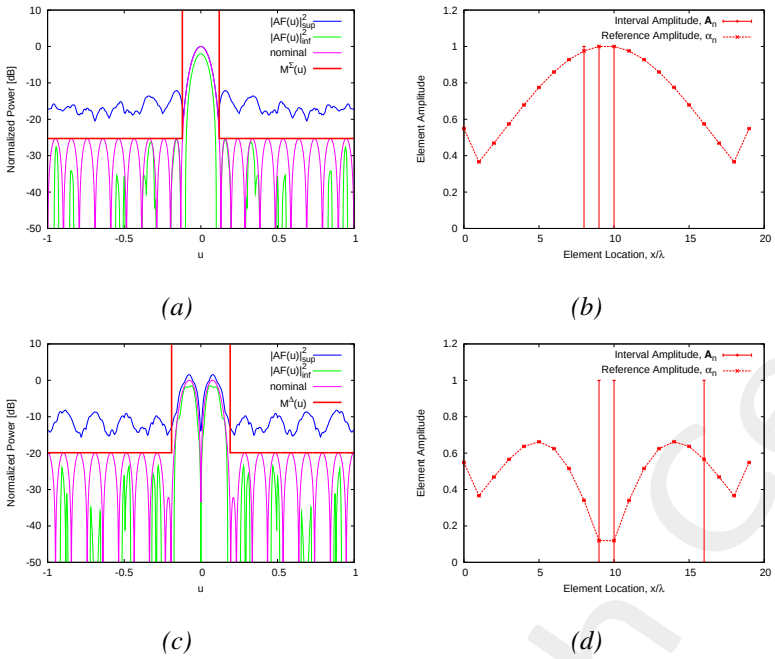

Figure 32. Radiation patterns *(a)(c)* and amplitudes *(b)(d)* for the worst sum beam *(a)(b)* and difference beam *(c)(d)* in terms of SLL.

- $P = 8$

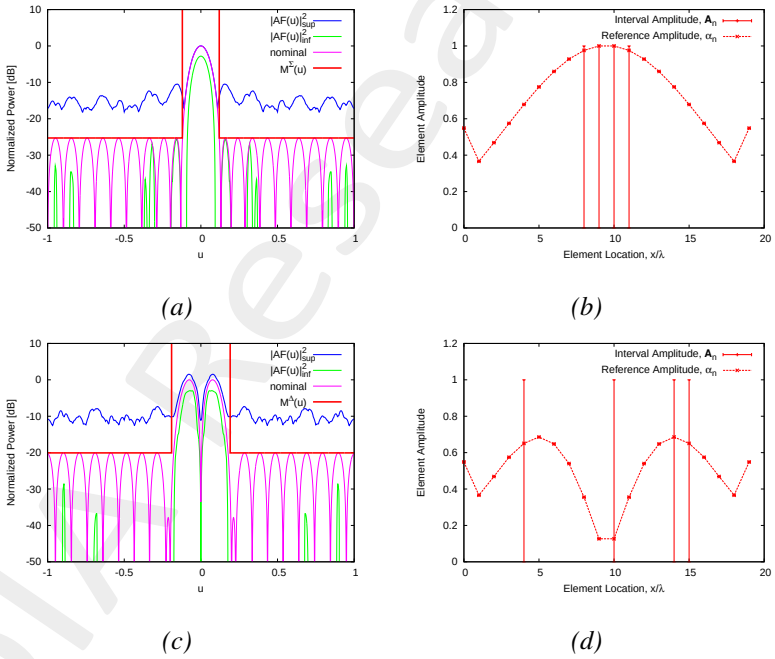

Figure 33. Radiation patterns *(a)(c)* and amplitudes *(b)(d)* for the worst sum beam *(a)(b)* and difference beam *(c)(d)* in terms of SLL.

BW:

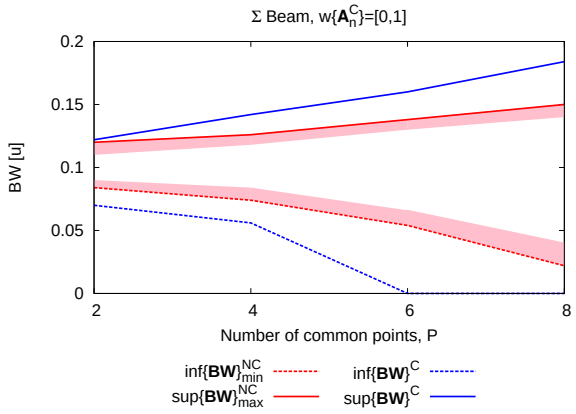

Figure 34. Sum Pattern $\mathbf{BW}$ vs P

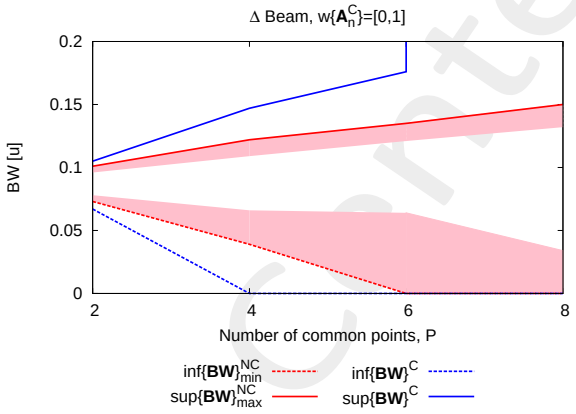

Figure 35. Difference Pattern $\mathbf{BW}$ vs P

P	$\inf\{\mathbf{BW}\}^{C}$	$\sup\{\mathbf{BW}\}^{C}$	$\inf\{\mathbf{BW}\}^{NC}_{min}$	$\inf\{\mathbf{BW}\}^{NC}_{max}$	$\sup\{\mathbf{BW}\}^{NC}_{min}$	$\sup\{\mathbf{BW}\}^{NC}_{max}$
2	0.07	0.122	0.084	0.09	0.11	0.12
4	0.056	0.142	0.074	0.084	0.118	0.126
6	0.0	0.16	0.054	0.066	0.13	0.138
8	0.0	0.184	0.022	0.04	0.14	0.15

Table 3. Sum Pattern $\mathbf{BW}$ values

P	$\inf\{\mathbf{BW}\}^{C}$	$\sup\{\mathbf{BW}\}^{C}$	$\inf\{\mathbf{BW}\}^{NC}_{min}$	$\inf\{\mathbf{BW}\}^{NC}_{max}$	$\sup\{\mathbf{BW}\}^{NC}_{min}$	$\sup\{\mathbf{BW}\}^{NC}_{max}$
2	0.067	0.105	0.073	0.078	0.096	0.101
4	0.0	0.147	0.039	0.066	0.109	0.122
6	0.0	0.176	0.0	0.064	0.121	0.135
8	0.0	4.0	0.0	0.034	0.132	0.15

Table 4. Difference Pattern $\mathbf{BW}$ values

WORST CASES:

In the following the patterns and excitations of the worst cases in terms of $\sup\{\mathbf{BW}\}_{max}^{NC}$ are reported.

- $P = 2$

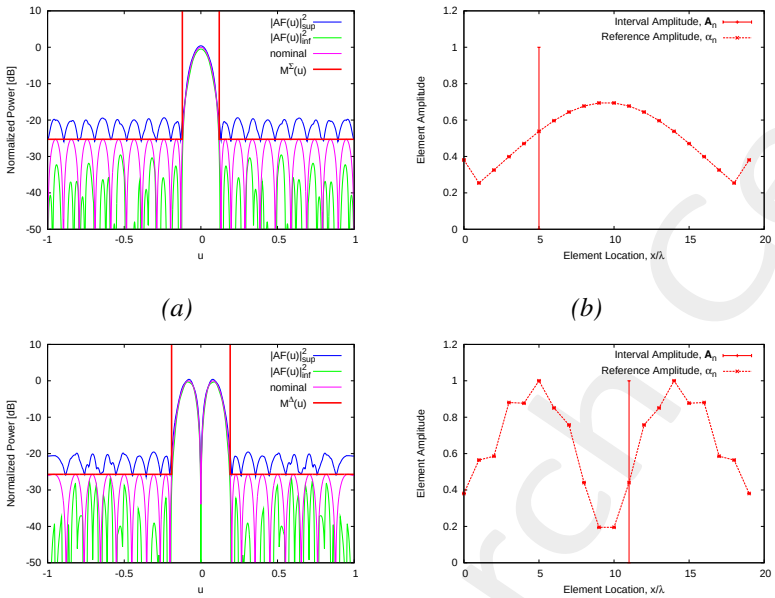

(a) *(b)*

(c) *(d)*

Figure 36. Radiation patterns *(a)(c)* and amplitudes *(b)(d)* for the worst sum beam *(a)(b)* and difference beam *(c)(d)* in terms of BW.

- $P = 4$

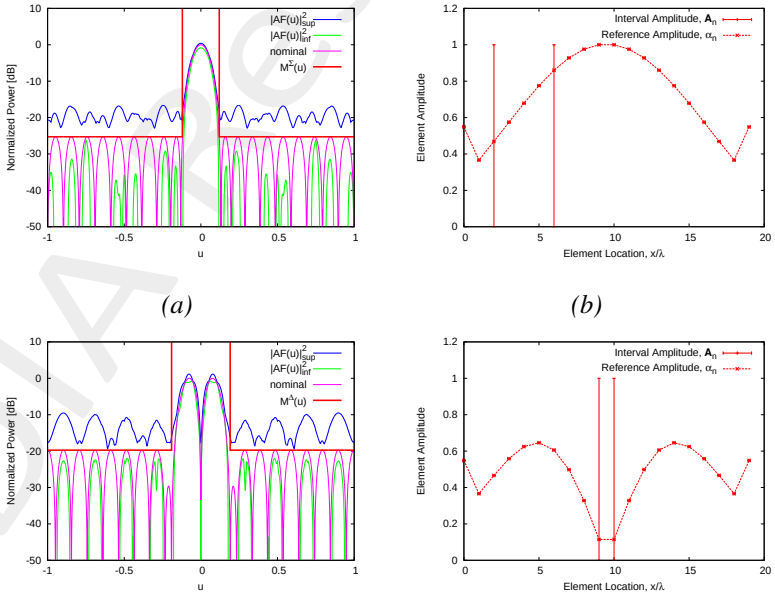

(a) *(b)*

(c) *(d)*

Figure 37. Radiation patterns *(a)(c)* and amplitudes *(b)(d)* for the worst sum beam *(a)(b)* and difference beam *(c)(d)* in terms of BW.

- $P = 6$

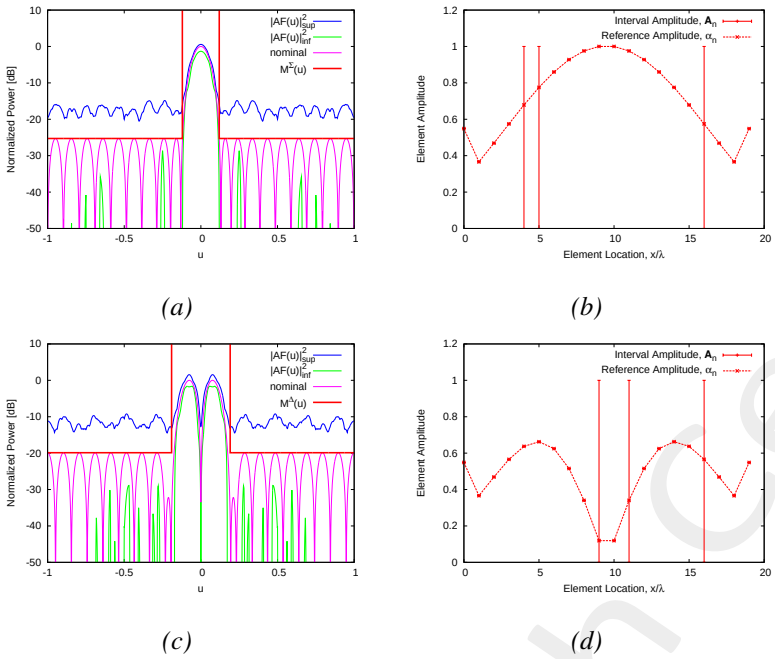

(a) *(b)*

(c) *(d)*

Figure 38. Radiation patterns *(a)(c)* and amplitudes *(b)(d)* for the worst sum beam *(a)(b)* and difference beam *(c)(d)* in terms of BW.

- $P = 8$

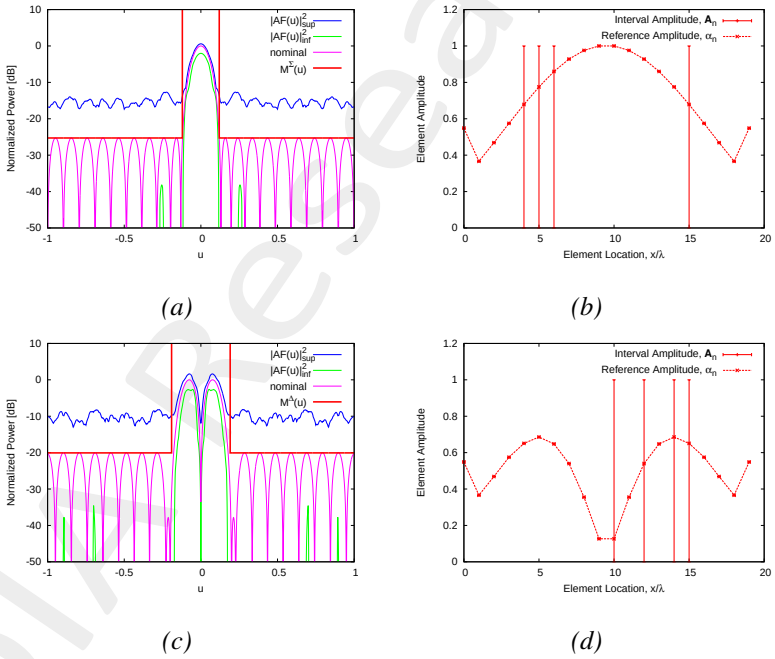

(a) *(b)*

(c) *(d)*

Figure 39. Radiation patterns *(a)(c)* and amplitudes *(b)(d)* for the worst sum beam *(a)(b)* and difference beam *(c)(d)* in terms of BW.

Remembering that:

- $$\chi_{\{\cdot\}} = \left(\sup\{\cdot\}^{\Sigma}_{max} - \inf\{\cdot\}^{\Sigma}_{min}\right) + \left(\sup\{\cdot\}^{\Delta}_{max} - \inf\{\cdot\}^{\Delta}_{min}\right) \quad (6)$$

where $\sup / \inf\{\cdot\}_{max}$ is the maximum $\sup / \inf$ among all the considered combination of faulty elements; $\sup / \inf\{\cdot\}_{min}$ is the respective minimum value.

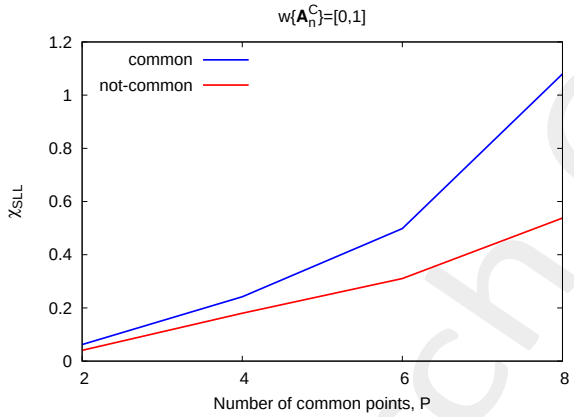

Figure 40. The χ_{SLL} relative to the SLL descriptor is plotted, for the common and not-common cases

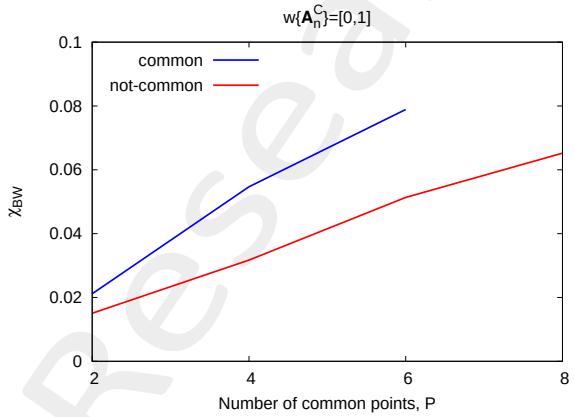

Figure 41. The χ_{BW} relative to the BW descriptor is plotted, for the common and not-common cases

1.4 Resume

Worst Cases in terms of SLL

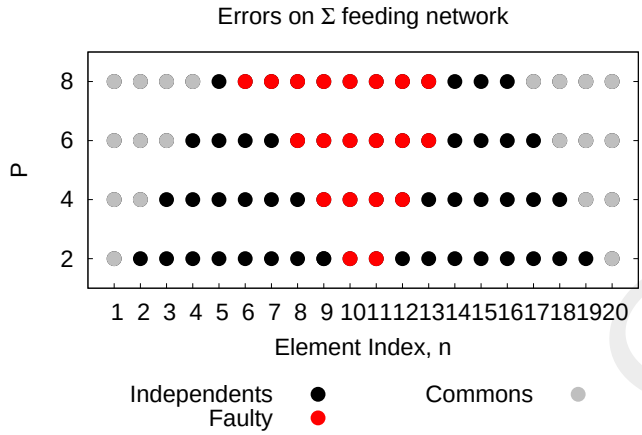

Figure 42. Worst case configurations in terms of SLL considering errors on the Σ beam network.

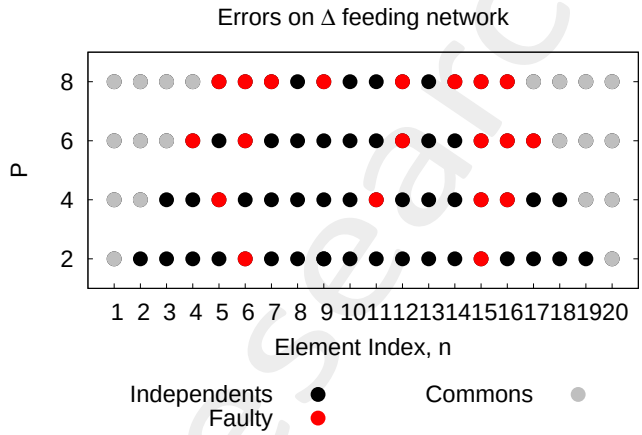

Figure 43. Worst case configurations in terms of SLL considering errors on the Δ beam network.

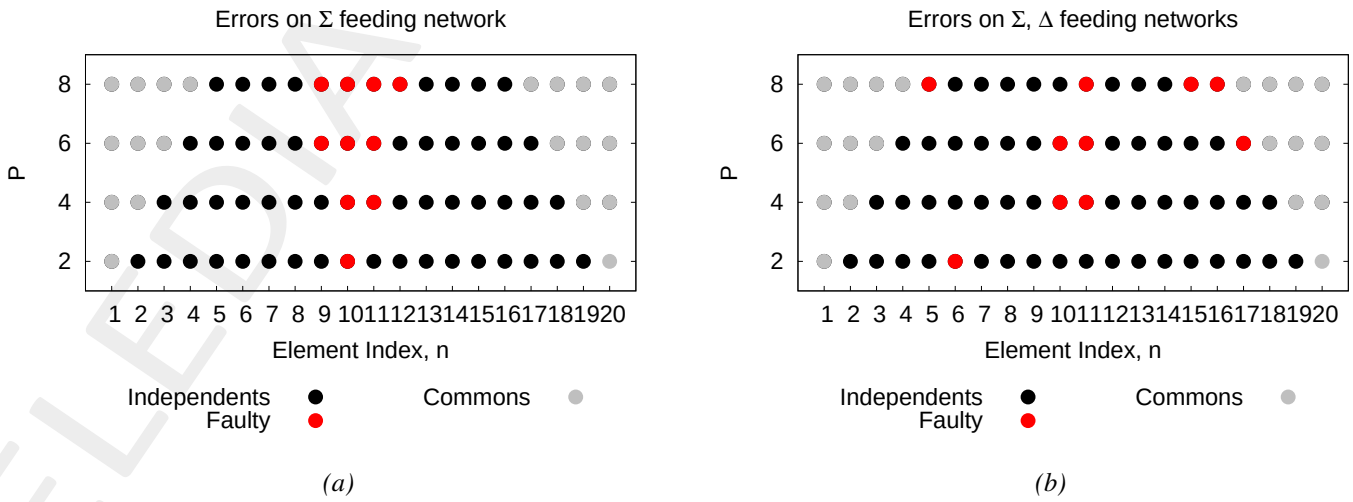

Figure 44. Worst case configurations in terms of SLL considering errors on the Σ *(a)* and Δ *(b)* feeding networks.

Worst Cases in terms of BW

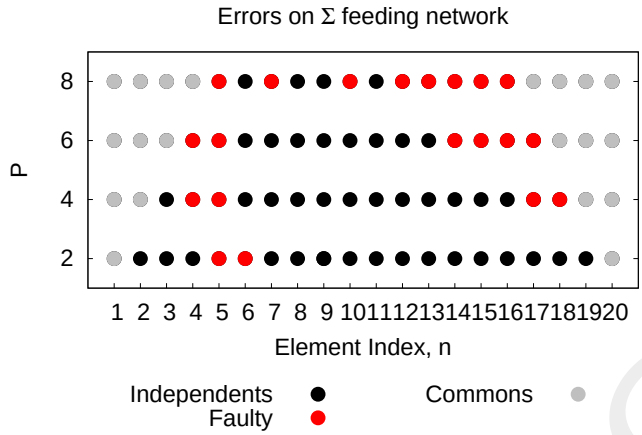

Figure 45. Worst case configurations in terms of BW considering errors on the Σ beam network.

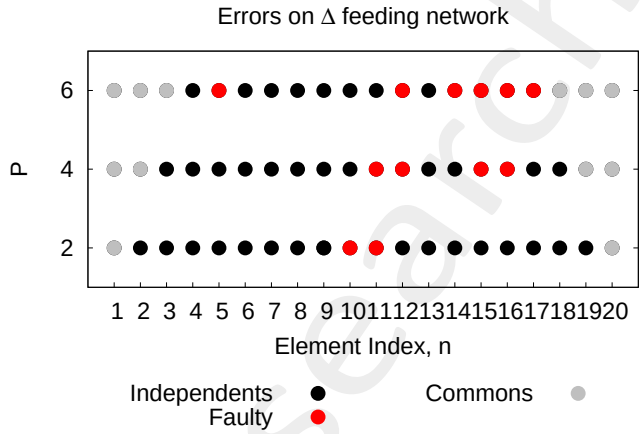

Figure 46. Worst case configurations in terms of BW considering errors on the Δ feeding network.

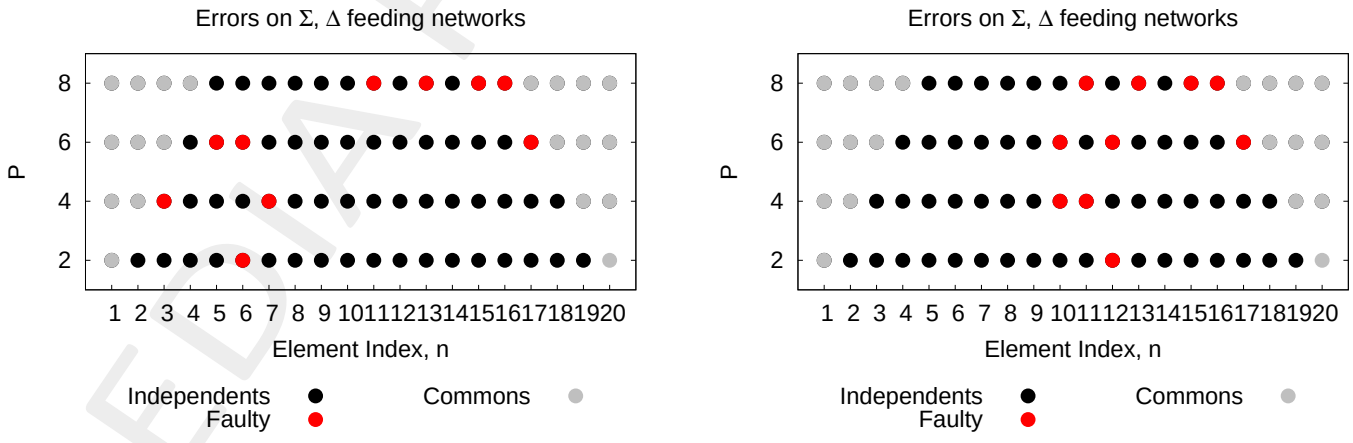

(a) *(b)*

Figure 47. Worst case configurations in terms of BW considering errors on the Σ *(a)* and Δ *(b)* feeding networks.

Comments on the results

In this paragraph we will put in evidence the criticality of the common points in a reconfigurable feeding network for linear antenna arrays. We can take as example the case in which 6 control points are in common. We have seen that with IA we can predict the system performances considering intervals over the $P = 6$ faulty control points, with a width that cover the entire normalized amplitude range, i.e. the amplifiers can assume whatever values between $[0,\ 1]$.

Let us analyze the performances of the SLL when the $P = 6$ common control points are faulty (Figure 7-8, blue lines), and when the $P = 6$ faulty elements belongs to the sum beam feeding network among the not-common elements (we are considering all the possible combination of P faulty elements among the Q not common elements). (Figure 7-8, red lines).

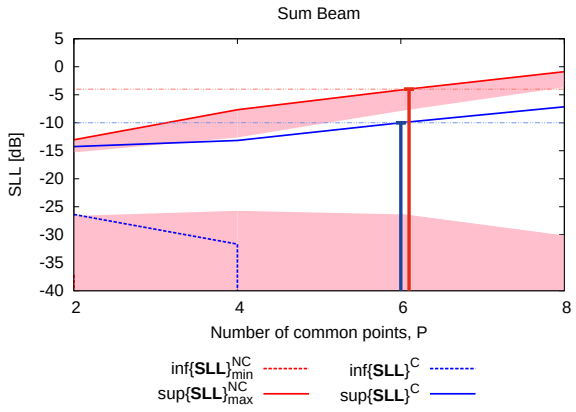

Figure 48. Sum Pattern **SLL** vs P

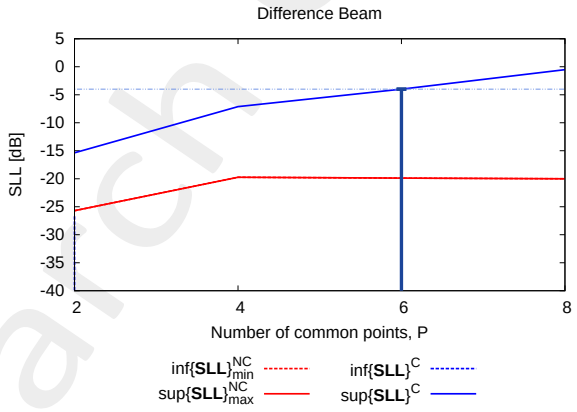

Figure 49. Difference Pattern **SLL** vs P

From Figure 7 we can see that the upper bound of the SLL of the sum beam can reach values up to $-10dB$ in case of faulty common elements; in the same time it raises up to $-4dB$ in case of not-common faulty elements, i.e. the sum beam radiation pattern performances are affected by the faulty elements in both cases. From Figure 8, we can see that, while the difference beam SLL upper bound can reach $-4dB$ in case of faulty common points, the performances of the difference beam SLL are not affected by the not-common faulty elements, i.e. the difference beam performances are deteriorated only in case of common faulty elements.

This underlines how the choice to reduce the number of the amplifiers, putting in common two or more control points of the feeding network, leads to a vulnerability of the systems performances on both the afforded radiation patterns, in case the elements are faulty. Moreover raising the number of common control points leads to a decrease in the performances.

Concluding, the derived graphs point out that we have to consider a tread-off between the complexity of the feeding network (number of common amplifiers) and the robustness of the common control points (cost of each common amplifier).

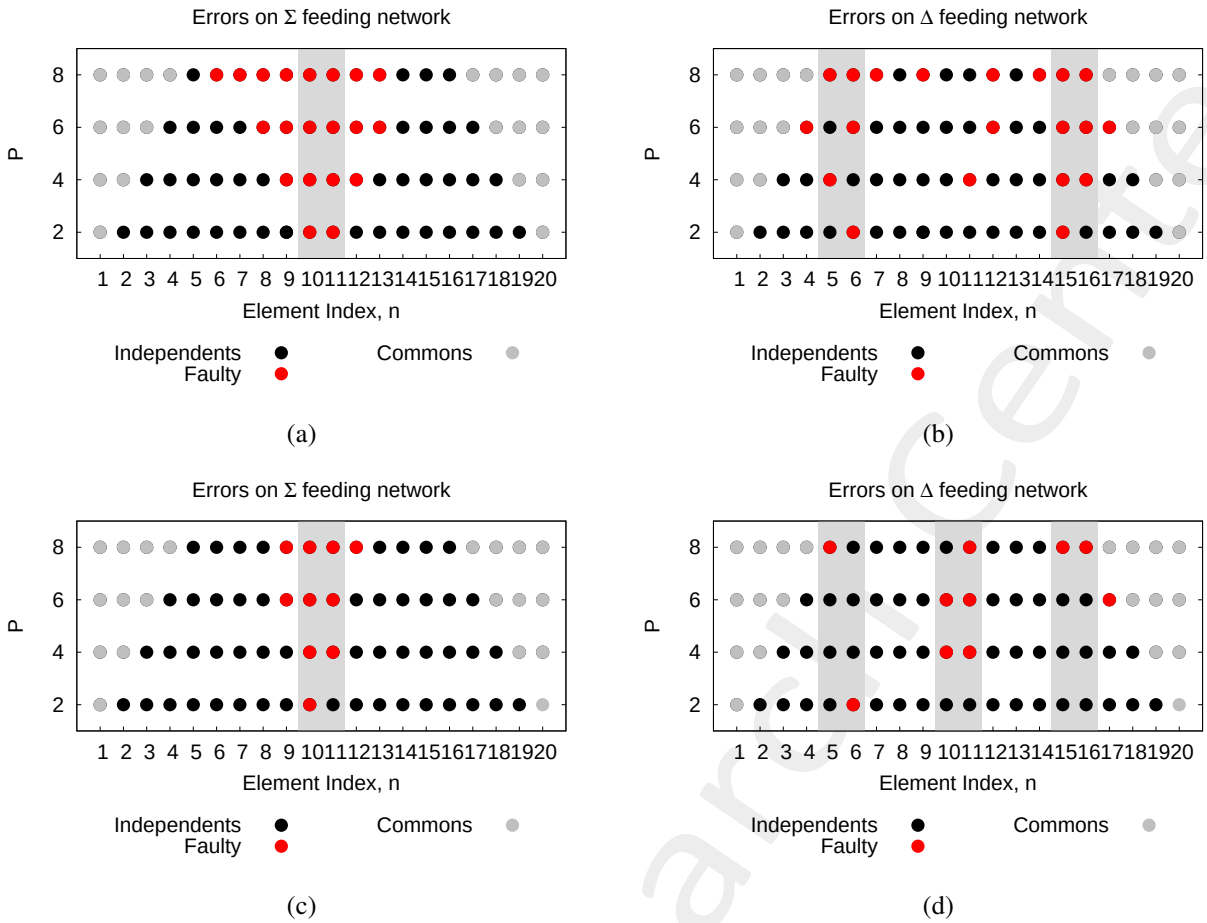

Figure 50. Worst case configurations in terms of SLL, errors on Σ (a), on Δ (b), and on both networks, considering the SLL performances on the Σ beam (a)(c) and on the Δ beam (b)(d).

Let us now trying to understand the criticality of the independent elements in terms of SLL. From the analysis of this section turns out that considering errors separately on the two independent beamforming networks the most critical elements are, the central elements in case of faulty elements on the Σ network, i.e. the ones with element index $n \in \{10, 11\}$ and in the neighboring. On the other side considering errored elements on the Δ network the most sensible elements are the one with element index $n \in \{5, 6, 15, 16\}$. In Fig. 9 the most critical elements are put in evidence by gray regions. It is worth noting that in these regions the excitations amplitudes assume the maximum values. Now let us considering the case in which the faulty elements are equally distributed among the two feeding networks. In this case the most critical regions are the same of the previous cases but now we need to add one more region, i.e. when the performances are computed on the Δ beam also the elements with indexes $n \in \{10, 11\}$ seams to be critical, even if these elements assume the minimum amplitude value. It is natural to conclude that one explanation can be that the most critical elements are the ones with the maximum or minimum value among the amplitudes distribution.

Pareto Front

Remembering that:

$$\zeta_{\{\cdot\}} = \sup\{\cdot\}_{max} - \inf\{\cdot\}_{min} \tag{7}$$

where $\sup / \inf\{\cdot\}_{max}$ is the maximum $\sup / \inf$ among all the considered combination of faulty elements; $\sup / \inf\{\cdot\}_{min}$ is the respective minimum value.

SLL:

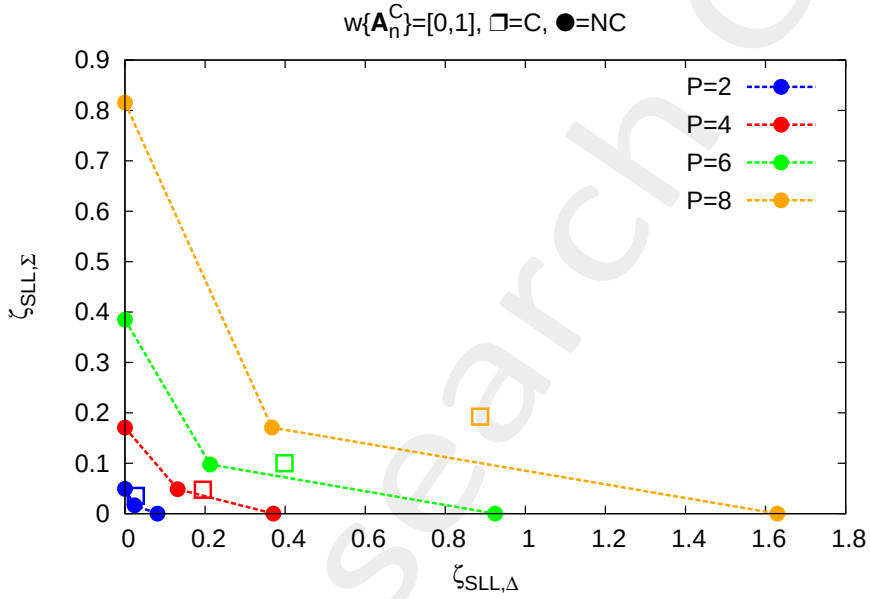

Figure 9. ζ values of the SLL, plotted in the Σ/Δ plane, when faulty elements occours on common (SQUARE) and independent (CIRCLE) elements

Observations:

- In Figure 9 we can see how, considering faulty elements on the $\Sigma - BFN$ or on the $\Delta - BFN$ ("circles" on the x/y axis) we obtain always worst performances in terms of SLL with respect to the common faulty elements case ("squares"). Anyway, when faulty elements occurs on independents elements, the performances of only one of the two beams will be affected.
- It's worth noting that considering the case of P faulty common elements ("squares"), leads to almost the same results in terms of Σ beam's performances with respect to the common faulty elements case equally distributed on both networks ("circles" on the diagonal) . In the same time Δ beam's performances are worst.

More information on the topics of this document can be found in the following list of references.

References

[1] G. Ding, N. Anselmi, W. Xu, P. Li, and P. Rocca, "Interval-bounded optimal power pattern synthesis of array antenna excitations robust to mutual coupling," *IEEE Antennas Wireless Propag. Lett.*, vol. 22, no. 11, pp. 2725-2729, Nov. 2023.

[2] N. Anselmi, P. Rocca, and A. Massa, "Tolerance analysis of reconfigurable monopulse linear antenna arrays through interval arithmetic," *J. Electromagn. Waves Appl. J*, pp. 1066-1081, 2023.

[3] P. Rocca, N. Anselmi, A. Benoni, and A. Massa, "Probabilistic interval analysis for the analytic prediction of the pattern tolerance distribution in linear phased arrays with random excitation errors," *IEEE Trans. Antennas Propag.*, vol. 68, no. 2, pp. 7866-7878, Dec. 2020.

[4] L. Tenuti, N. Anselmi, P. Rocca, M. Salucci, and A. Massa, "Minkowski sum method for planar arrays sensitivity analysis with uncertain-but-bounded excitation tolerances" *IEEE Trans. Antennas Propag.*, vol. 65, no. 1, pp. 167-177, Jan. 2017.

[5] N. Anselmi, P. Rocca, M. Salucci, and A. Massa, "Optimization of excitation tolerances for robust beamforming in linear arrays," *IET Microwaves, Antennas & Propagation*, vol. 10, no. 2, pp. 208-214, 2016.

[6] N. Anselmi, P. Rocca, M. Salucci, and A. Massa, "Power pattern sensitivity to calibration errors and mutual coupling in linear arrays through circular interval arithmetics," *Sensors*, vol. 16, no. 6 (791), pp. 1-14, 2016.

[7] L. Poli, P. Rocca, N. Anselmi, and A. Massa, "Dealing with uncertainties on phase weighting of linear antenna arrays by means of interval-based tolerance analysis," *IEEE Trans. Antennas Propag.*, vol. 63, no. 7, pp. 3299-3234, Jul. 2015.

[8] P. Rocca, N. Anselmi, and A. Massa, "Optimal synthesis of robust array configurations exploiting interval analysis and convex optimization," *IEEE Trans. Antennas Propag.*, vol. 62, no. 7, pp. 3603-3612, July 2014.

[9] T. Moriyama, L. Poli, N. Anselmi, M. Salucci, and P. Rocca, "Real array pattern tolerances from amplitude excitation errors," *IEICE Electronics Express*, vol. 11, no. 17, pp. 1-8, Sep. 2014.

[10] N. Anselmi, L. Manica, P. Rocca, and A. Massa, "Tolerance analysis of antenna arrays through interval arithmetic," *IEEE Trans. Antennas Propag.*, vol. 61, no. 11, pp. 5496-5507, Nov. 2013.

[11] L. Manica, N. Anselmi, P. Rocca, and A. Massa, "Robust mask-constrained linear array synthesis through an interval-based particle swarm optimisation," *IET Microwaves, Antennas and Propagation*, vol. 7, no. 12, pp. 976-984, Sep. 2013.

[12] P. Rocca, L. Manica, N. Anselmi, and A. Massa, "Analysis of the pattern tolerances in linear arrays with arbitrary amplitude errors," *IEEE Antennas Wireless Propag. Lett.*, vol. 12, pp. 639-642, 2013.

[13] L. Manica, P. Rocca, N. Anselmi, and A. Massa, "On the synthesis of reliable linear arrays through interval arithmetic," *IEEE International Symposium on Antennas Propag. (APS/URSI 2013)*, *Orlando, Florida*, *USA*, Jul. 7-12, 2013.

[14] L. Manica, P. Rocca, G. Oliveri, and A. Massa, "Designing radiating systems through interval analysis tools," *IEEE International Symposium on Antennas Propag. (APS/URSI 2013), Orlando, Florida, USA*, Jul. 7-12, 2013.

[15] M. Carlin, N. Anselmi, L. Manica, P. Rocca, and A. Massa, "Exploiting interval arithmetic for predicting real arrays performances - The linear case," *IEEE International Symposium on Antennas Propag. (APS/URSI 2013), Orlando, Florida, USA*, Jul. 7-12, 2013.

[16] N. Anselmi, M. Salucci, P. Rocca, and A. Massa, "Generalised interval-based analysis tool for pattern distortions in reflector antennas with bump-like surface deformations," *IET Microwaves, Antennas & Propagation*, vol. 10, no. 9, p. 909-916, June 2016.

[17] P. Rocca, L. Poli, N. Anselmi, M. Salucci, and A. Massa, "Predicting antenna pattern degradations in microstrip reflectarrays through interval arithmetic," *IET Microwaves, Antennas & Propagation*, vol. 10, no. 8, pp. 817-826, May 2016.

[18] P. Rocca, L. Manica, and A. Massa, "Interval-based analysis of pattern distortions in reflector antennas with bump-like surface deformations," *IET Microwaves, Antennas and Propagation*, vol. 8, no. 15, pp. 1277-1285, Dec. 2014.

[19] P. Rocca, N. Anselmi, and A. Massa, "Interval Arithmetic for pattern tolerance analysis of parabolic reflectors," *IEEE Trans. Antennas Propag.*, vol. 62, no. 10, pp. 4952-4960, Oct. 2014.